Scientific Research Publishing

Open Journal of Applied Sciences, 2025, 15(2), 411-424
https://www.scirp.org/journal/ojapps
ISSN Online: 2165-3925
ISSN Print: 2165-3917

Determination of Fracture Plane Orientation Using the Variance Method under Multiaxial Loading

Mbaiyelkom Esdras[1], Ngargueudedjim Kimtangar[1*], Bianzeube Tikri[1], Kenmeugne Bienvenu[2], Fogue Médard[3]

[1]Laboratoire d'Etude et de Recherche en Technique Industrielles (LERTI), Faculté des Sciences Exactes et Appliquées, Université de N'Djaména, N'Djaména, Chad
[2]Laboratoire d'Engineering Civil et Mécanique (LECM), Ecole Nationale Supérieure Polytechnique de Yaoundé, Université de Yaoundé I, Yaoundé, Cameroun
[3]Unité de Recherche d'Ingénierie des Systèmes Industriels et de l'Environnement (UR-ISIE), Faculté des Sciences, Université de Dschang, Dschang, Cameroun
Email: mbaiyelkom@gmail.com, *kimta_ernest@yahoo.fr, bitikri@gmail.com, kenmeugneb@gmail.com, medar_fog@yahoo.com

How to cite this paper: Esdras, M., Kimtangar, N., Tikri, B., Bienvenu, K. and Médard, F. (2025) Determination of Fracture Plane Orientation Using the Variance Method under Multiaxial Loading. *Open Journal of Applied Sciences*, **15**, 411-424.
https://doi.org/10.4236/ojapps.2025.152026

Received: January 16, 2025
Accepted: February 17, 2025
Published: February 20, 2025

Copyright © 2025 by author(s) and Scientific Research Publishing Inc.
This work is licensed under the Creative Commons Attribution International License (CC BY 4.0).
http://creativecommons.org/licenses/by/4.0/

Open Access

Abstract

The prediction of the fracture plane orientation in fatigue is a scientific topic and remains relevant for every type of material. However, in this work, we compared the orientation of the fracture plane obtained experimentally through tests on specimens under multiaxial loading with that calculated by the variance method. In the statistical approach criteria, several methods have been developed but we have presented only one method, namely the variance method using the equivalent stress. She assumes that the fracture plane orientation is the one on which the variance of the equivalent stress is maximum. Three types of equivalent stress are defined for this method [1]: normal stress, shear stress and combined normal and shear stress. The results obtained were compared with experimental results for multiaxial cyclic stress states, and it emerges that the variance method for the case of combined loading is conservative as it gives a better prediction of the fracture plane.

Keywords

Biaxial Fatigue, Fracture Plane Orientation, Critical Fracture Plane, Variance Method, Fatigue Criteria

1. Introduction

Estimating the fatigue life of mechanical components or structures in service un-

der complex loading (multiple and random) is a major concern in mechanical engineering today. To be competitive, the industrial purpose is to guarantee the safety of users of their products, without losing sight of the need to minimize manufacturing and maintenance costs.

Statistical criteria are insufficient for the dimensioning of structural parts for validation in the design office. That's why, in recent years, many researchers and engineers have been working on theoretical and experimental fatigue models. Predicting the fatigue life [2] of mechanical components subjected to varied loading is the primary goal of materials fatigue research.

In fatigue models, determining the orientation of the fracture plane is crucial since it's necessary to compute the fatigue life. This paper's ultimate goal is to use test data from the Polish laboratory [3] to compare the calculated fatigue fracture plane orientation with the experimental one.

2. Materials and Method

2.1. Method

Presentation of the Variance Method

Under the two assumptions below, Macha, E. and Niesłony [3] have developed a method for determining the position of the critical plane based on the variance of the equivalent stress.

Fatigue fracture is caused by the normal stresses $\sigma_\eta(t)$ and the shear stresses $\tau_\eta(t)$ acting in the $\vec{s}$ direction on a fracture plane with a normal $\vec{\eta}$ (**Figure 1**). $\sigma_\eta(t)$ and $\tau_\eta(t)$ are functions of the components of contrainte $\sigma_{ij}(t)$ ($i, j = x, y; z$).

The direction $\vec{s}$ on the fracture plane coincides with the mean value of the shear stress maximale $\tau_{\eta\max}(t)$ (**Figure 2**).

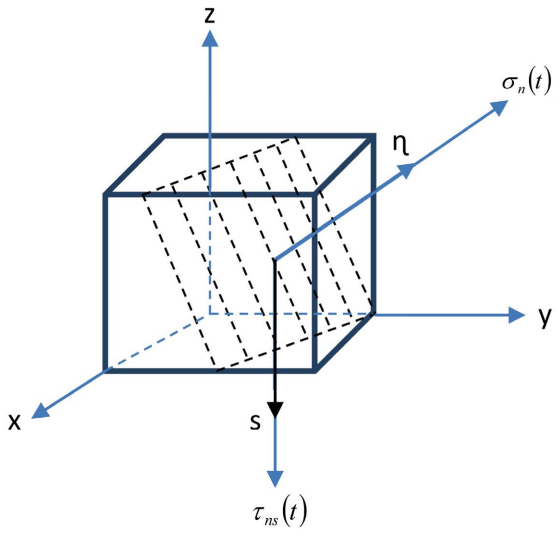

Figure 1. Direction of vectors $\vec{\eta}$ and $\vec{s}$ and of stresses $\sigma_\eta(t)$, $\tau_\eta(t)$ in the case where the fatigue fracture plane can point in any direction [3] [4].

With:

$$\vec{n} = \hat{l}_\eta \vec{i} + \hat{m}_\eta \vec{j} + \hat{n}_{\eta\vec{k}} = \frac{\hat{l}_1 + \hat{l}_3}{\sqrt{2}} \vec{i} + \frac{\hat{m}_1 + \hat{m}_3}{\sqrt{2}} \vec{j} + \frac{\hat{n}_1 + \hat{n}_3}{\sqrt{2}} \vec{k} \tag{1}$$

$$\vec{s} = \hat{l}_s \vec{i} + \hat{m}_s \vec{j} + \hat{n}_s \vec{k} = \frac{\hat{l}_1 - \hat{l}_3}{\sqrt{2}} \vec{i} + \frac{\hat{m}_1 - \hat{m}_3}{\sqrt{2}} \vec{j} + \frac{\hat{n}_1 - \hat{n}_3}{\sqrt{2}} \vec{k} \tag{2}$$

The components of the stress vector are expressed as:

$$\vec{\sigma}_n(t) = \hat{l}_n \vec{i} \hat{l}_n \vec{j} \sigma_{ij}(t), \quad \vec{\tau}_{ns}(t) = \hat{l}_{ns} \vec{i} \hat{l}_{ns} \vec{j} \sigma_{ij}(t) \tag{3}$$

In the proposed algorithm, the multiaxial stress state is reduced to an equivalent uniaxial stress state. The general formulation of the criterion is:

$$\max_t \left\{ B\tau_{\eta s}(t) + K\sigma_\eta(t) \right\} = F \quad [5] \tag{4}$$

where *F*, *B*, *K* are the constants for selection of a special version of the criterion:

Cas a) criterion of maximum normal stress on the critical plane (*B* = 0, *K* = 1)

The equivalent stress expression is:

$$\begin{aligned} \sigma_{eq}(t) &= \sigma_\eta(t) = \sigma_{eq}(t) \\ &= \hat{l}_\eta^2 \sigma_{xx}(t) + \hat{m}_\eta^2 \sigma_{xx}(t) + \hat{n}_\eta^2 \sigma_{xx}(t) + 2\hat{l}_\eta \hat{m}_\eta \sigma_{xy}(t) \\ &\quad + 2\hat{l}_\eta \hat{n}_\eta \sigma_{xz}(t) + 2\hat{m}_\eta \hat{n}_\eta \sigma_{yz}(t) \end{aligned} \tag{5}$$

Cas b) criterion of maximum shear stress on the critical plane (*B* = 1, *K* = 0)

$$\begin{aligned} \sigma_{eq}(t) &= 2\tau_{\eta s}(t) \\ &= 2\hat{l}_\eta \hat{l}_s \sigma_{xx}(t) + 2\hat{m}_\eta \hat{m}_s \sigma_{yy}(t) + 2\hat{n}_\eta \hat{n}_s \sigma_{zz}(t) \\ &\quad + 2\left(\hat{l}_\eta \hat{m}_s + \hat{l}_s \hat{m}_\eta\right) \sigma_{xy}(t) + 2\left(\hat{l}_\eta \hat{n}_s + \hat{l}_s \hat{n}_\eta\right) \sigma_{xz}(t) \\ &\quad + 2\left(\hat{m}_\eta \hat{n}_s + \hat{m}_s \hat{n}_\eta\right) \sigma_{yz}(t) \end{aligned} \tag{6}$$

Cas c) Criterion of maximum normal and shear stress on the critical plane (*B* = 1)

$$\begin{aligned} \sigma_{eq}(t) = \frac{1}{1+K} \Big[& \left(\hat{l}_1^2 - \hat{l}_3^2 + K\left(\hat{l}_1 + \hat{l}_3\right)^2 \right) \sigma_{xx}(t) \\ & + \left(\hat{m}_1^2 - \hat{m}_3^2 + K\left(\hat{m}_1 + \hat{m}_3\right)^2 \right) \sigma_{yy}(t) \\ & + \left(\hat{n}_1^2 - \hat{n}_3^2 + K\left(\hat{n}_1 + \hat{n}_3\right)^2 \right) \sigma_{zz}(t) \\ & + 2\left(\hat{l}_1 \hat{m}_1 - \hat{l}_3 \hat{m}_3 + K\left(\hat{l}_1 + \hat{l}_3\right)\left(\hat{m}_1 + \hat{m}_3\right) \right) \sigma_{xy}(t) \\ & + 2\left(\hat{l}_1 n_1 - \hat{l}_3 \hat{n}_3 + K\left(\hat{l}_1 + \hat{l}_3\right)\left(\hat{n}_1 + \hat{n}_3\right) \right) \sigma_{xz}(t) \\ & + 2\left(\hat{m}_1 \hat{n}_1 - \hat{n}_3 \hat{m}_3 + K\left(\hat{m}_1 + \hat{m}_3\right)\left(\hat{n}_1 + \hat{n}_3\right) \right) \sigma_{yz}(t) \Big] \end{aligned} \tag{7}$$

The equivalent stress can be understood as the output signal from the linear physical system with six inputs, where the signals representing suitable compo-

nents of the stress tensor were delivered. Then the equivalent history can be determinned by summation of the products of suitable components tensor $x_k(t)$ and coefficients a_k.

$$\sigma_{eq}(t) = \sum_{k=1}^{6} a_k x_k(t) \tag{8}$$

where: $x_1 = \sigma_{xx}(t)$, $x_2 = \sigma_{yy}(t)$, $x_3 = \sigma_{zz}(t)$, $x_4 = \sigma_{xy}(t)$, $x_5 = \sigma_{xz}(t)$, $x_6 = \sigma_{yz}(t)$.

and $a_k = a_k\left(\hat{l}_1, \hat{m}_1, \hat{n}_1, \hat{l}_3, \hat{m}_3, \hat{n}_3\right)$.

The variance of the equivalent stress is written as:

$$\mu_{\sigma_{eq}} = \sum_{s,t=1}^{6} a_s a_t \mu_{xst} \quad [6] \tag{9}$$

With μ_{xst} [7] the variance-covariance matrix of the variable x_k:

$$\mu_{xst} = \begin{bmatrix} \mu_{x11} & \cdots & \mu_{16} \\ \vdots & \ddots & \vdots \\ \mu_{61} & \cdots & \mu_{66} \end{bmatrix}$$

Generally, the analytical resolution of this method poses a problem then, to eliminate this difficulty, the cosines direction $\hat{l}_n, \hat{m}_n, \hat{n}_n$ are replaced by the trigonometric functions of the three Euler angles ψ, θ, ϕ (**Figure 2**).

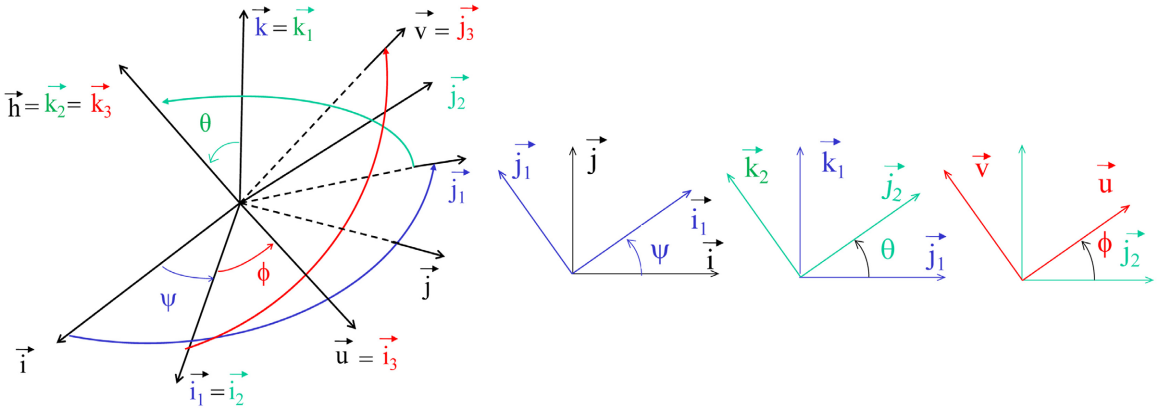

Figure 2. Euler angles.

Considering that the problem is planar and the facets concerned are those with the normal in the plane $(\vec{i}, \vec{j})$, we have the condition $\vec{k} \cdot \vec{h} = \hat{n}_3 = 0$.

With the condition $\theta = \pi/2$, we have the following matrix of cosine directions:

The algorithm for determining the fracture plane is shown in detail in **Figure 3**.

$$[P] = \begin{bmatrix} \cos\psi\cos\phi & \cos\psi\sin\phi & \sin\phi \\ -\sin\psi\cos\phi & -\sin\psi\sin\phi & \cos\psi \\ \sin\phi & -\cos\phi & 0 \end{bmatrix}$$

2.2. Material Presentation

To validate this comparative study for determining the orientation of the fracture

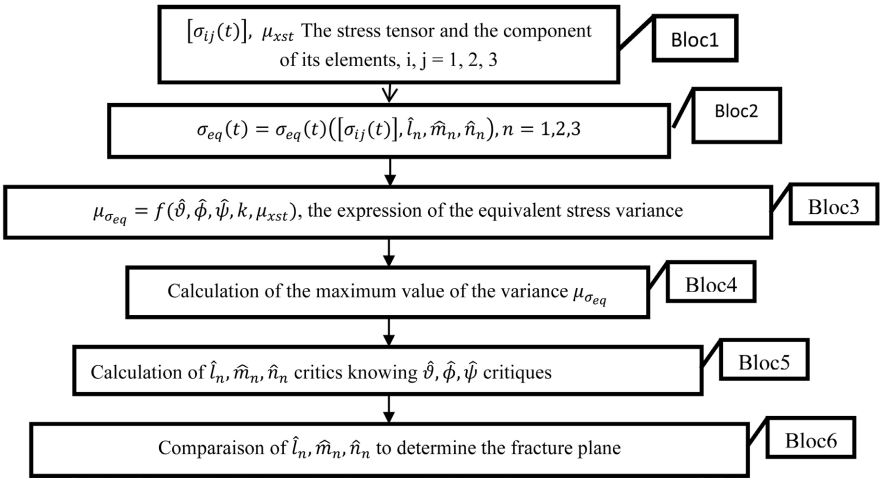

Figure 3. Algorithme of fracture plane determination.

plane, we used fatigue data from structural steel and fatigue tests under cyclic bi-axial loading carried out by Rotvel [8], Nishihara T. and Kawamoto [9] and Achtelik *et al*. [10] (**Table 1**).

Table 1. Cyclic stress states and fatigue data [2]-[5].

Authors: [8] [11]		
	Chemical properties (%)	Mechanical properties
Cylindrical specimens under tension-compression stress states Material: carbon steel	C = 0.35. Si = 0.20. Mn = 0.45	σ_{-1} = 215.8 MPa, σ_0 = 349.9 MPa, τ_{-1} = 138.5 MPa, *Rm* = 570 MPa
Stress states		
Test number	$\sigma_{xx}(t)$	$\sigma_{xy}(t)$
1	227.6sin(*wt*)	1.96sin(*wt*)
2	−2.94 + 224.6sin(*wt*)	6.87sin(*wt* + π)
3	52 + 233.5sin(*wt*)	41.2 + 191.3sin(*wt*)
4	−11.8 + 228.6sin(*wt*)	−24.5 + 117.7sin(*wt*)
5	−7.8 + 156sin(*wt*)	11.77 + 121.6sin(*wt* + π)
6	79.5 + 155sin(*wt* + π)	118.7sin(*wt*)

Authors: [9] [11].		
	Chemical properties (%)	Mechanical properties
Round specimens under complex bending and torsion Material: carbon Hardened steel	C = 0.51, Mn = 0.38, S = 0.010, Si = 0.27, P = 0.023	σ_{-1} = 313.9 MPa, σ_0 = 485.8 MPa, τ_{-1} = 196.2 MPa, *Rm* = 694 MPa
Stress states		

Continued

Test number	$\sigma_{xx}(t)$	$\tau_{xy}(t)$
HNK50	00	225.63sin(wt)
HNK53	353.16sin(wt)	00
HNK54	00	sin(wt)
HNK55	323.73sin(wt)	00
HNK59	294.30sin($wt + \pi/2$)	147.15sin(wt)
HNK60	274.68sin(wt)	137.34sin(wt)
HNK63	264.87sin($wt + \pi/2$)	132.44sin(wt)
HNK67	162.85sin($wt + \pi/2$)	196.69sin(wt)
HNK69	154.45sin($wt + \pi/2$)	184.23sin(wt)
HNK74	162.85sin(wt)	195.69sin(wt)
HNK75	308.03sin(wt)	63.86sin(wt)
HNK76	141.85sin(wt)	171.28sin(wt)
HNK79	344.33sin(wt)	71.32sin(wt)
HNK83	344.33sin($wt + \pi/2$)	71.32sin(wt)
HNK84	157.65sin($wt + \pi/3$)	190.31sin(wt)
HNK86	308.03sin($wt + \pi/3$)	63.86sin(wt)
HNK89	255.06sin(wt)	127.53sin(wt)
HNK90	264.87sin($wt + \pi/3$)	132.44sin(wt)
HNK91	255.06sin($wt + \pi/3$)	127.53sin(wt)
HNK94	147.15sin($wt + \pi/3$)	177.56sin(wt)
HNK96	141.95sin($wt + \pi/6$)	171.18sin(wt)
HNK97	152.35sin($wt + \pi/6$)	183.94sin(wt)

Authors: [9] [11].			
		Chemical properties (%)	Mechanical properties
Round specimens under complex bending and torsion Material: carbon mild steel		C = 0.1, Mn = 0.50, S = 0.040, Si = 0.14, P = 0.033	σ_{-1} = 235.4 MPa, σ_0 = 325.7 MPa, τ_{-1} = 137.3 MPa, Rm = 382 MPa
Stress states			
N˚	Test number	$\sigma_{xx}(t)$	$\sigma_{xy}(t)$
1	LNK5	194.3sin(wt)	00
2	LNK11	00	142.25sin(wt)
3	LNK12	187.12sin(wt)	93.50sin(wt)
4	LNK16	101.34sin(wt)	122.33sin(wt)
5	LNK18	235.64sin(wt)	48.85sin(wt)

Continued

6	LNK22	235.83sin($wt + \pi/2$)	117.92sin(wt)
7	LNK24	208.07sin($wt + \pi/2$)	104.08sin(wt)
8	LNK27	112.62sin($wt + \pi/2$)	135.97sin(wt)
9	LNK28	244.76sin($wt + \pi/2$)	50.72sin(wt)
10	LNK29	235.64sin($wt + \pi/2$)	48.85sin(wt)
11	LNK31	201.11sin($wt + \pi/3$)	100.55sin(wt)
12	LNK32	194.24sin($wt + \pi/3$)	97.12sin(wt)
13	LNK35	245.25sin(wt)	00
14	LNK36	105.16sin($wt + \pi/3$)	126.84sin(wt)
15	LNK40	108.89sin($wt + \pi/3$)	131.45sin(wt)

Authors: [9] [11].		
	Chemical properties (%)	Mechanical properties
Round specimens under complex bending and torsion Material: duraluminium	Cu = 3.81, Mn = 0.44, Si = 0.35	σ_{-1} = 156 MPa, σ_0 = 257.1 MPa, τ_{-1} = 100 MPa, Rm = 443 MPa

Stress states			
N˚	Test number	σ_{11a}	σ_{12a}
01	D-30 2	00	98.1sin(ωt)
02	D-30 5	00	127.53sin(ωt)
03	D-30 6	156.96sin(ωt)	00
04	D-30 7	196.2sin($\omega t + \pi/2$)	00
05	D-30 8	181.29sin($\omega t + \pi/2$)	37.57sin(ωt)
06	D-30 12	153.55sin(ωt)	76.32sin(ωt)
07	D-30 15	138.7($\omega t + \pi/2$)	69.36sin(ωt)
08	D-30 16	124.88sin(ωt)	62.49sin(ωt)
09	D-30 17	163.14sin(ωt)	33.75sin(ωt)
10	D-30 19	117.92($\omega t + \pi/2$)	58.96sin(ωt)
11	D-30 20	82.6sin(ωt)	99.67sin(ωt)
12	D-30 22	199.44sin(ωt)	41.3sin(ωt)
13	D-30 23	199.44sin($\omega t + \pi/2$)	41.3sin(ωt)
14	D-30 24	82.6sin($\omega t + \pi/2$)	99.67sin(ωt)

Authors: [10] [11].		
	Chemical properties (%)	Mechanical properties

Continued

Round specimens under bending-torsion stress states Material: Grey Cast iron	C = 3.32%	σ_{-1} = 143 MPa, σ_0 = 212.7 MPa τ_{-1} = 110 MPa, Rm = 278.8

		Stress states	
N°	Test number	σ_{11a}	σ_{12a}
01	Zla1	168sinωt	00sinωt
02	Zla2	164sinωt	00sinωt
03	Zla3	160sinωt	00sinωt
04	Zlb1	00 sinωt	142sinωt
05	Zlb2	00 sinωt	130sinωt
06	Zlb3	00 sinωt	132sinωt
07	Zlc1	149.9sinωt	74.95sinωt
08	Zlc2	121.62sinωt	60.81sinωt
09	Zlc3	118.79sinωt	59.4sinωt
10	Zld1	176.67sinωt	51sinωt
11	Zld2	155.88sinωt	45sinωt
12	Zld3	152.42sinωt	44sinωt
13	Zle1	118sinωt	102.2sinωt
14	Zle2	108sinωt	93.53sinωt
15	Zle3	106sinωt	91.78sinωt

3. Results and Discussion

3.1. Results

The experimental fracture plane is defined by the unit normal vector $\overrightarrow{\boldsymbol{h}_{ex}}$. The predicted fracture planes are defined by the theoretical unit normal vector $\overrightarrow{\boldsymbol{h}_{t1}}$. In the case where several assessed fracture planes is obtained, the most similar to that obtained experimentally is assumed. The closeness of the corresponding cosines directions $\hat{l}_{nex}, \hat{m}_{nex}$ and $\hat{l}_{nc}, \hat{m}_{nc}$ is suitability of the predicting methods. The dot product of this unit vector is calculated to express the agreement (or disagreement) between assessments and tests results.

Table 2 shows the direction of cosines experimentally and calculated.

The criterion for comparison is the percentage number of results.

3.2. Discussion

Figures 4-6 give us a summary of the previous results. In view of the results shown in Table 2, the variance method for the case of combined loading (case c) gives a very good result in terms of predicting the orientation of the fracture plane. It produces better predictions for tests on carbon steel at 0.35% C, hardened steel at 0.51% C, soft steel at 0.1% C, Grey Cast iron at 3.32 Cu, and duralumin at 3.81%

Table 2. Expérimental and predicted fracture plane orientation (cyclic stress states).

Test number	Experimental cosines directions		Theoretical cosines directions in the fracture plane position								
			Variance method								
			Cas a			Cas b			Cas c		
	$\hat{l}_{nex}$	$\hat{m}_{nex}$	$\hat{l}_{nt1}$	$\hat{m}_{nt1}$	$\overrightarrow{h_{ex}} \cdot \overrightarrow{h_{t1}}$	$\hat{l}_{nt1}$	$\hat{m}_{nt1}$	$\overrightarrow{h_{ex}} \cdot \overrightarrow{h_{t1}}$	$\hat{l}_{nt1}$	$\hat{m}_{nt1}$	$\overrightarrow{h_{ex}} \cdot \overrightarrow{h_{t1}}$
1	1.00	0.00	−0.58	0.81	**−0.58**	0.58	0.81	**0.58**	0.96	0.28	**0.96**
2	1.00	0.00	−0.57	0.82	**−0.58**	0.82	0.57	**0.82**	0.96	0.29	**0.96**
3	1.00	0.00	−0.15	0.99	**−0.15**	0.57	−0.42	**0.57**	0.80	0.61	**0.80**
4	1.00	0.00	−0.43	0.90	**−0.43**	0.66	−0.24	**0.66**	0.91	0.41	**0.91**
5	1.00	0.00	−0.08	1.00	**−0.08**	0.54	−0.46	**0.54**	0.76	0.65	**0.76**
6	1.00	0.00	−0.37	0.93	**−0.37**	0.65	−0.28	**0.65**	0.90	0.45	**0.90**
Number of plans close to experimental ones				**0**			**0**			**4**	
Percentage of admissible efficiency				**0.00%**			**0.00%**			**66.67%**	

Test number		Experimental cosines directions		Theoretical cosines directions in the fracture plane position								
				Variance method								
				Cas a			Cas b			Cas c		
		$\hat{l}_{nex}$	$\hat{m}_{nex}$	$\hat{l}_{nt1}$	$\hat{m}_{nt1}$	$\overrightarrow{h_{ex}} \cdot \overrightarrow{h_{t1}}$	$\hat{l}_{nt1}$	$\hat{m}_{nt1}$	$\overrightarrow{h_{ex}} \cdot \overrightarrow{h_{t1}}$	$\hat{l}_{nt1}$	$\hat{m}_{nt1}$	$\overrightarrow{h_{ex}} \cdot \overrightarrow{h_{t1}}$
1	HNK50	0.71	0.71	0.00	1.00	**0.71**	1.00	**0.00**	**0.71**	**0.71**	**−0.71**	**0.00**
2	HNK53	1.00	0.00	−0.59	0.81	**−0.59**	0.81	0.59	**0.81**	**0.96**	−0.26	**0.96**
3	HNK54	0.71	0.71	0.00	1.00	**0.71**	1.00	**0.00**	**0.71**	**0.71**	**−0.71**	**0.00**
4	HNK55	1.00	0.00	−0.59	0.81	**−0.59**	0.81	0.59	**0.81**	**0.96**	−0.26	**0.96**
5	HNK59	1.00	0.00	0.85	−0.52	**0.85**	0.85	−0.52	**0.85**	0.95	0.32	**0.95**
6	HNK60	0.92	0.38	0.85	−0.52	**0.58**	0.85	−0.52	**0.58**	0.95	0.32	**0.99**
7	HNK63	1.00	0.00	0.85	−0.52	**0.85**	0.85	−0.52	**0.85**	0.95	0.32	**0.95**
8	HNK67	0.91	0.41	0.96	−0.26	**0.77**	0.96	−0.26	**0.77**	0.85	0.52	**0.99**
9	HNK69	0.88	0.47	0.96	−0.27	**0.72**	0.96	−0.27	**0.72**	0.86	0.51	**1.00**
10	HNK74	0.82	0.57	0.96	−0.26	**0.64**	0.96	−0.26	**0.64**	0.85	0.52	**0.99**
11	HNK75	0.98	0.19	0.71	−0.70	**0.56**	0.71	−0.70	**0.56**	0.99	0.13	**0.99**
12	HNK76	0.83	0.56	0.96	−0.26	**0.65**	0.96	−0.26	**0.65**	0.85	0.52	**1.00**
13	HNK79	0.98	0.19	0.71	−0.70	**0.56**	0.71	−0.70	**0.56**	0.99	0.13	**0.99**
14	HNK83	1.00	0.00	0.71	−0.70	**0.71**	0.71	−0.70	**0.71**	0.99	0.13	**0.99**
15	HNK84	0.92	0.39	0.96	−0.26	**0.78**	0.96	−0.26	**0.78**	0.85	0.52	**0.98**
16	HNK86	1.00	0.00	0.71	−0.70	**0.71**	0.71	−0.70	**0.71**	0.99	0.13	**0.99**
17	HNK89	0.93	0.37	0.85	−0.52	**0.60**	0.85	−0.52	**0.60**	0.95	0.32	**1.00**

Continued

18	HNK90	0.85	0.53	0.85	−0.52	**0.45**	0.85	−0.52	**0.45**	0.95	0.32	**0.98**
19	HNK91	0.92	0.39	0.85	−0.52	**0.58**	0.85	−0.52	**0.58**	0.95	0.32	**1.00**
20	HNK94	0.93	0.37	0.96	−0.26	**0.80**	0.96	−0.26	**0.80**	0.85	0.52	**0.98**
21	HNK96	0.85	0.53	0.96	−0.26	**0.68**	0.96	−0.26	**0.70**	0.85	0.52	**1.00**
22	HNK97	0.92	0.39	0.96	−0.26	**0.78**	0.96	−0.26	**0.78**	0.85	0.52	**0.98**
23	HNK98	0.93	0.37	0.85	−0.52	**0.60**	0.85	−0.52	**0.60**	0.95	0.32	**1.00**
24	HNK99	0.85	0.53	0.85	−0.52	**0.45**	0.85	−0.52	**0.45**	0.95	0.32	**0.98**
Number of plans close to experimental ones					**8**			**8**			**20**	
Percentage of admissible efficiency					**33.33%**			**33.33%**			**83.33%**	

Test number		**Experimental cosines directions**		**Theoretical cosines directions in the fracture plane position**								
				Variance method								
				Cas a			**Cas b**			**Cas c**		
		$\hat{l}_{nex}$	$\hat{m}_{nex}$	$\hat{l}_{nt1}$	$\hat{m}_{nt1}$	$\overrightarrow{h_{ex}} \cdot \overrightarrow{h_{t1}}$	$\hat{l}_{nt1}$	$\hat{m}_{nt1}$	$\overrightarrow{h_{ex}} \cdot \overrightarrow{h_{t1}}$	$\hat{l}_{nt1}$	$\hat{m}_{nt1}$	$\overrightarrow{h_{ex}} \cdot \overrightarrow{h_{t1}}$
1	LNK5	1.00	0.00	−0.59	0.81	**−0.59**	0.81	0.59	**0.81**	0.97	−0.23	**0.97**
2	LNK11	0.71	0.71	0.00	1.00	**0.71**	1.00	0.00	**0.71**	0.71	−0.71	**0.00**
3	LNK12	0.93	0.37	0.85	−0.53	**0.59**	0.85	−0.53	**0.59**	0.95	0.29	**0.99**
4	LNK16	0.87	0.49	0.96	−0.26	**0.71**	0.96	−0.26	**0.71**	0.86	0.51	**1.00**
5	LNK18	0.98	0.20	0.71	−0.70	**0.56**	0.71	−0.70	**0.56**	1.00	0.09	**1.00**
6	LNK22	0.99	0.14	0.85	−0.52	**0.77**	0.85	−0.52	**0.77**	0.95	0.29	**0.98**
7	LNK24	0.99	0.14	0.85	−0.52	**0.77**	0.85	−0.52	**0.77**	0.95	0.29	**0.98**
8	LNK27	0.78	0.63	0.96	−0.26	**0.59**	0.96	−0.26	**0.59**	0.86	0.51	**0.99**
9	LNK28	1.00	0.00	0.71	−0.70	**0.71**	0.71	−0.70	**0.71**	1.00	0.09	**1.00**
10	LNK29	1.00	0.00	0.71	−0.70	**0.71**	0.71	−0.70	**0.71**	1.00	0.09	**1.00**
11	LNK31	0.99	0.14	0.85	−0.52	**0.77**	0.85	−0.52	**0.77**	0.95	0.29	**0.98**
12	LNK32	0.98	0.20	0.85	−0.52	**0.73**	0.85	−0.52	**0.73**	0.95	0.29	**0.99**
13	LNK35	1.00	0.00	−0.59	0.81	**−0.59**	0.81	0.59	**0.81**	0.97	−0.23	**0.97**
14	LNK36	0.93	0.37	0.96	−0.26	**0.80**	0.96	−0.26	**0.80**	0.86	0.51	**0.99**
15	LNK40	0.99	0.14	0.96	−0.26	**0.91**	0.96	−0.26	**0.91**	0.86	0.51	**0.92**
Number of plans close to experimental ones					**5**			**5**			**13**	
Percentage of admissible efficiency					**33.33%**			**33.33%**			**86.67%**	

Test number		Experimental cosines directions		Theoretical cosines directions in the fracture plane position								
				Variance method								
				Cas a			Cas b			Cas c		
		$\hat{l}_{nex}$	$\hat{m}_{nex}$	$\hat{l}_{nt1}$	$\hat{m}_{nt1}$	$\overrightarrow{h_{ex}} \cdot \overrightarrow{h_{t1}}$	$\hat{l}_{nt1}$	$\hat{m}_{nt1}$	$\overrightarrow{h_{ex}} \cdot \overrightarrow{h_{t1}}$	$\hat{l}_{nt1}$	$\hat{m}_{nt1}$	$\overrightarrow{h_{ex}} \cdot \overrightarrow{h_{t1}}$
1	D-30 2	1.00	0.00	0.00	1.00	**0.00**	1.00	0.00	**1.00**	0.71	−0.71	**0.71**
2	D-30 5	1.00	0.00	0.00	1.00	**0.00**	1.00	0.00	**1.00**	0.71	−0.71	**0.71**
3	D-30 6	0.97	0.24	−0.59	0.81	**−0.78**	0.81	0.59	**0.93**	0.96	−0.28	**0.86**
4	D-30 7	0.98	0.20	−0.59	0.81	**−0.42**	0.81	0.59	**0.91**	0.96	−0.28	**0.88**
5	D-30 8	0.88	0.47	0.71	−0.70	**0.30**	0.71	−0.70	**0.30**	0.99	0.15	**0.94**
6	D-30 12	0.87	0.49	0.85	−0.52	**0.48**	0.53	0.85	**0.88**	0.94	0.33	**0.98**
7	D-30 15	1.00	0.00	0.85	−0.52	**0.85**	0.85	−0.52	**0.85**	0.94	0.33	**0.94**
8	D-30 16	0.82	0.57	0.85	−0.52	**0.40**	0.85	−0.52	**0.40**	0.94	0.33	**0.96**
9	D-30 17	0.80	0.60	0.71	−0.70	**0.15**	0.71	−0.70	**0.15**	0.99	0.15	**0.88**
10	D-30 19	1.00	0.00	0.85	−0.52	**0.85**	0.85	−0.52	**0.85**	0.94	0.33	**0.94**
11	D-30 20	1.00	0.00	0.96	−0.26	**0.96**	0.96	−0.26	**0.96**	0.85	0.52	**0.85**
12	D-30 22	0.82	0.57	0.71	−0.70	**0.18**	0.71	−0.70	**0.18**	0.99	0.15	**0.90**
13	D-30 23	0.85	0.53	0.71	−0.70	**0.18**	0.71	−0.70	**0.18**	0.99	0.15	**0.92**
14	D-30 24	1.00	0.00	0.96	−0.26	**0.96**	0.96	−0.26	**0.96**	0.85	0.52	**0.85**
Number of plans close to experimental ones				**7**			**9**			**11**		
Percentage of admissible efficiency				**50.00%**			**64.29%**			**78.57%**		

Test number		Experimental cosines directions		Theoretical cosines directions in the fracture plane position								
				Variance method								
				Cas a			Cas b			Cas c		
		$\hat{l}_{nex}$	$\hat{m}_{nex}$	$\hat{l}_{nt1}$	$\hat{m}_{nt1}$	$\overrightarrow{h_{ex}} \cdot \overrightarrow{h_{t1}}$	$\hat{l}_{nt1}$	$\hat{m}_{nt1}$	$\overrightarrow{h_{ex}} \cdot \overrightarrow{h_{t1}}$	$\hat{l}_{nt1}$	$\hat{m}_{nt1}$	$\overrightarrow{h_{ex}} \cdot \overrightarrow{h_{t1}}$
1	Zla1	1.00	0.00	−0.59	0.81	**−0.59**	0.81	0.59	**0.81**	0.93	−0.37	**0.93**
2	Zla2	1.00	0.00	−0.59	0.81	**−0.59**	0.81	0.59	**0.81**	0.93	−0.37	**0.93**
3	Zla3	1.00	0.00	−0.59	0.81	**−0.59**	0.81	0.59	**0.81**	0.93	−0.37	**0.93**
4	Zlb1	0.71	0.71	0.00	1.00	**0.71**	1.00	0.00	**0.71**	0.71	−0.71	**0.00**
5	Zlb2	0.71	0.71	0.00	1.00	**0.71**	1.00	0.00	**0.71**	0.71	−0.71	**0.00**
6	Zlb3	0.71	0.71	0.00	1.00	**0.71**	1.00	0.00	**0.71**	0.71	−0.71	**0.00**
7	Zlc1	0.88	0.47	0.85	−0.52	**0.50**	0.85	−0.52	**0.50**	0.91	0.41	**0.99**
8	Zlc2	0.88	0.47	0.85	−0.52	**0.50**	0.85	−0.52	**0.50**	0.91	0.41	**0.99**
9	Zlc3	0.91	0.42	0.85	−0.52	**0.55**	0.85	−0.52	**0.55**	0.91	0.41	**1.00**
10	Zld1	0.95	0.30	0.75	−0.65	**0.52**	0.65	0.75	**0.84**	0.95	0.32	**1.00**

Continued

11	Zld2	0.96	0.29	0.75	−0.65	**0.53**	0.65	0.75	**0.84**	0.95	0.32	**1.00**
12	Zld3	0.97	0.23	0.75	−0.65	**0.58**	0.65	0.75	**0.80**	0.95	0.32	**0.99**
13	Zle1	0.81	0.59	0.93	−0.36	**0.54**	0.36	0.93	**0.84**	0.86	0.50	**0.99**
14	Zle2	0.80	0.60	0.93	−0.36	**0.53**	0.36	0.93	**0.85**	0.86	0.50	**0.99**
15	Zle3	0.82	0.57	0.93	−0.36	**0.56**	0.36	0.93	**0.82**	0.86	0.50	**0.99**
Number of plans close to experimental ones				**0**			**0**			**4**		
Percentage of admissible efficiency				**0.00%**			**0.00%**			**26.67%**		

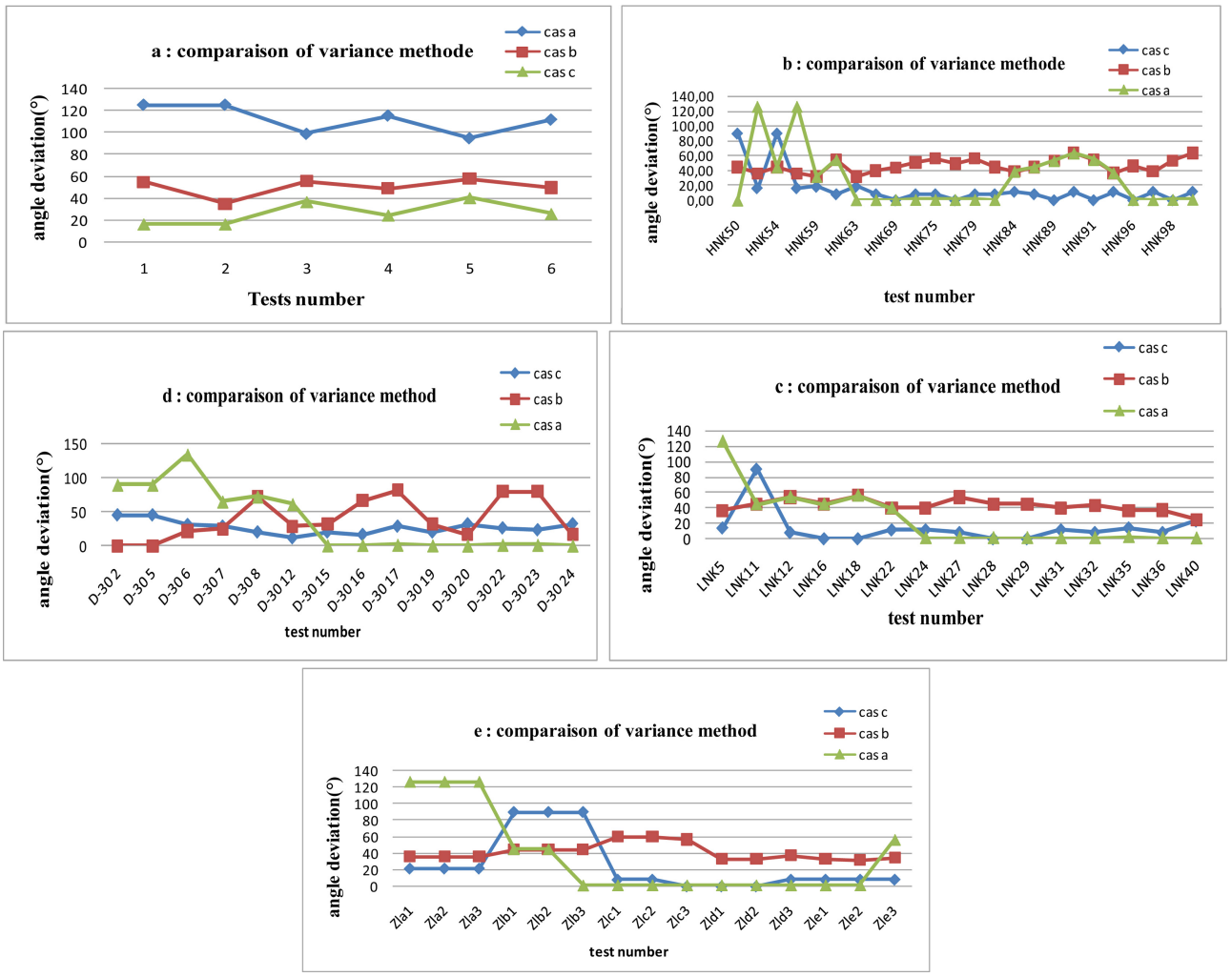

Figure 4. Angles deviations between predicted and experimental fracture plane orientations.

C than cases a and b. The overall mean value of the dot product is about 0.68 for cas c, 0.26 cas b and 0.23 for cas a (Figure 5). It indicates average deviation angles of 20.37, 42.38 and 31.99 respectively of the deviation between predicted fracture

planes against the real ones (Figure 6). Figure 7 shows us the distribution of critical planes according to the direction cosines.

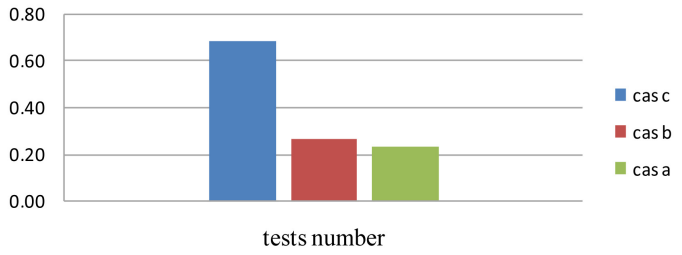

Figure 5. Overall mean value of the dot product.

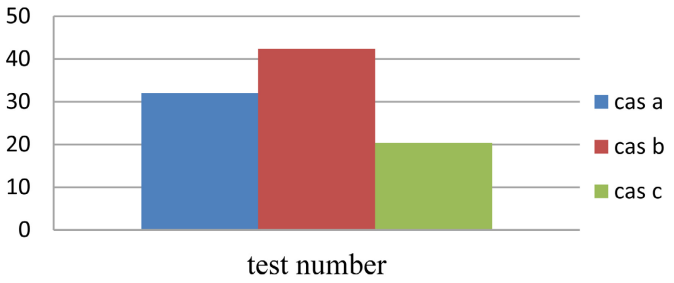

Figure 6. Average deviation angles.

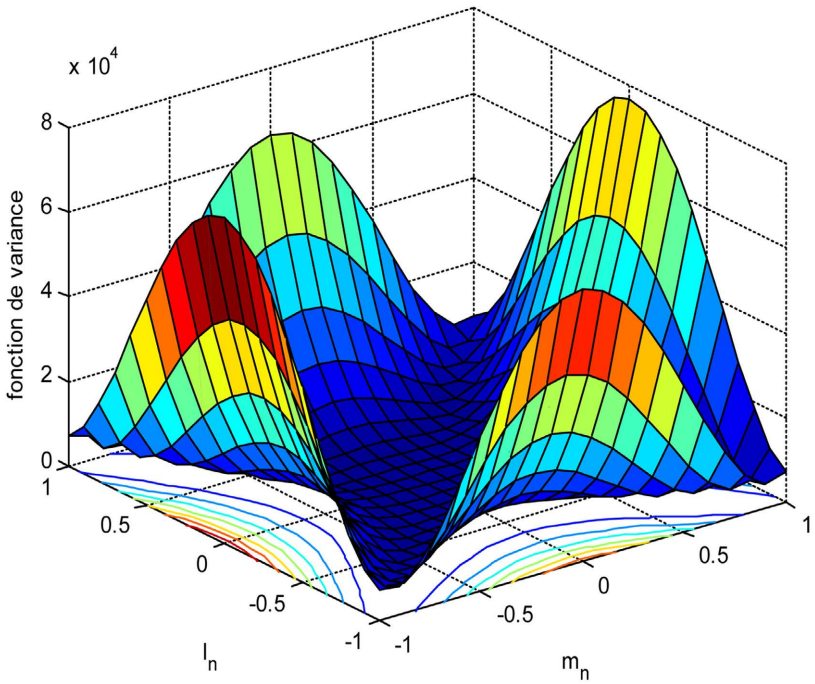

Figure 7. Variance function for case c.

4. Conclusion

Fracture plane predictions from different variance method formulations have been compared with experimental results for a biaxial cyclic stress condition.

Based on the results obtained, we can conclude that for the material types—carbon steel with 0.35% C, hardened steel with 0.51% C, soft steel with 0.1% C, and grey cast iron with 3.32% C—the variance method, when applied to the case of combined loading, is conservative. It provides a better prediction of the fracture plane, with accuracies of 66.67%, 83.33%, 86.67%, 78.57%, and 26.67% respectively for each material type.

Conflicts of Interest

The authors declare no conflicts of interest regarding the publication of this paper.

References

[1] Macha, E. (1989) Simulation Investigations of the Position of Fatigue Fracture Plane in Materials with Biaxial Loads. *Materialwissenschaft und Werkstofftechnik*, **20**, 132-136. https://doi.org/10.1002/mawe.19890200405

[2] Kenmeugne, B. (1996) Contribution à la modélisation du comportement en fatigue sous sollicitations multiaxiales d'amplitude variable. Master's Thesis, Lyon INSA.

[3] Macha, E. and Niesłony, A. (2012) Critical Plane Fatigue Life Models of Materials and Structures under Multiaxial Stationary Random Loading: The State-of-the-Art in Opole Research Centre CESTI and Directions of Future Activities. *International Journal of Fatigue*, **39**, 95-102. https://doi.org/10.1016/j.ijfatigue.2011.03.001

[4] Macha, E. (1989) Generalization of Fatigue Fracture Criteria for Multiaxial Sinusoidal Loadings in the Range of Random Loadings. *Biaxial and Multiaxial Fatigue*, *EGF*, **3**, 425-436.

[5] Będkowski, W. and Macha, E. (1992) Fatigue Fracture Plane under Multiaxial Random Loadings—Prediction by Variance of Equivalent Stress Based on the Maximum Shear and Normal Stresses. *Materialwissenschaft und Werkstofftechnik*, **23**, 82-94. https://doi.org/10.1002/mawe.19920230305

[6] Bedkowski, W. (1994) Determination of the Critical Plane and EFFORT criterion in Fatigue Life Evaluation for Materials under Multiaxial Random Loading. Experimental Verification Based on Fatigue Tests of Cruciform Specimens. Societe Francaise de Metallurgie et de Materiaux (France), 435-447.

[7] Lachowicz, C.T., Łagoda, T. and Macha, E. (1992) Covariance between Components of Biaxial Stress State in Fatigue Life Calculations. *Materialwissenschaft und Werkstofftechnik*, **23**, 201-212. https://doi.org/10.1002/mawe.19920230604

[8] Rotvel, F. (1970) Biaxial Fatigue Tests with Zero Mean Stresses Using Tubular Specimens. *International Journal of Mechanical Sciences*, **12**, 597-613. https://doi.org/10.1016/0020-7403(70)90091-3

[9] Nishihara, T. and Kawamoto, M. (1945) The Strength of Metals under Combined Alternating Bending and Torsion with Phase Difference. *Memoirs of the College of Engineering*, *Kyoto Imperial University*, **XI**, 95-112.

[10] Achtelik, H., Jakubowska, I. and Macha, E. (1983) Actual and Estimated Directions of Fatigue Fracture Plane in ZI250 Grey Cast Iron under Combined Alternating Bending and Torsion. *Studia Geotechnica et Mechanica*, **5**, 9-30.

[11] Będkowski, W., Weber, B., Macha, E. and Robert, J. (1999) Comparison of Variance and Damage Indicator Methods for Prediction of the Fracture Plane Orientation in Multiaxial Fatigue. *European Structural Integrity Society*, **25**, 147-165. https://doi.org/10.1016/s1566-1369(99)80013-2